SOOTING LIMITS OF MICROGRAVITY SPHERICAL DIFFUSION FLAMES

P. B. SUNDERLAND[1], D. L. URBAN[2], D. P. STOCKER[2],
B. -H. CHAO[3], and R. L. AXELBAUM[4]

[1]National Center for Microgravity Research
[1,2]NASA Glenn Research Laboratory
Cleveland OH 44135, USA
[3]Department of Mechanical Engineering
University of Hawaii at Manoa
Honolulu HI 96822, USA
[4]Department of Mechanical Engineering
Washington University
St. Louis MO 63130, USA

Submitted to:
29th International Symposium on Combustion

Submission Date:
December 13, 2001

Suggested Colloquium:
Pollutant Formation and Control (NOx, SOx, PAH, Soot, Air Toxics)

Running Title:
Sooting Limits

Word Count:
Body – 4146
References – 189
Table 1 – 200
Figures 1-5 – 1000
Total – 5535

Corresponding Author:
Richard L. Axelbaum
Washington University
305 Jolly Hall
St. Louis MO 63130 USA
(314) 935-7560, fax: (314) 935-4014
rla@mecf.wustl.edu

ABSTRACT

Limiting conditions for soot-particle inception were studied in microgravity spherical diffusion flames burning ethylene at atmospheric pressure. Nitrogen was supplied in the fuel and/or oxidizer to obtain the broadest range of stoichiometric mixture fraction. Both normal flames (oxygen in ambience) and inverted flames (fuel in ambience) were considered. Microgravity was obtained in the NASA Glenn 2.2-second drop tower. The flames were observed with a color video camera and sooting conditions were defined as conditions for which yellow emission was present throughout the duration of the drop. Sooting limit results were successfully correlated in terms of adiabatic flame temperature and stoichiometric mixture fraction. Soot free conditions were favored by increased stoichiometric mixture fractions. No statistically significant effect of convection direction on sooting limits was observed. The relationship between adiabatic flame temperature and stoichiometric mixture fraction at the sooting limits was found to be in qualitative agreement with a simple theory based on the assumption that soot inception can occur only where temperature and local C/O ratio exceed threshold values (circa 1250 K and 1, respectively).

Introduction

Soot formation in flames is an active research area because of its significance and complexity, as discussed in the reviews of Refs. [1-3]. Soot may be responsible for more deaths than any other air pollutant [4] and its presence in practical combustors can lead to performance penalties. The aim of this work is to advance the understanding of soot by identifying the fundamental limits of soot particle inception in diffusion flames.

Many fundamental sooting limits have come from studies of laminar premixed flames [1,2,5-8]. One reason for this success is that the C/O mole ratio and temperature are nearly constant in the soot forming regions of premixed flames. Sooting limits in premixed flames typically are identified by the equivalence ratio (or, alternatively, the effective equivalence ratio or the C/O mole ratio) at which luminous yellow emission is barely perceptible. Sooting limits in laminar premixed flames depend on fuel type, equivalence ratio, amount and type of inert, and, weakly, pressure. These limits are intrinsic properties of the mixtures and they offer both practical value

and important information about soot inception processes in premixed flames. A sooting limit with a high C/O ratio for a given flame temperature indicates a greater amount of carbon is needed to form soot, and thus the conditions, e.g. fuel type, are less conducive to forming soot. Takahashi and Glassman [5] concluded that premixed-flame sooting limits result from a competition between fuel pyrolysis and oxidative attack. Markatou et al. [7] found that the oxidation that is critical to sooting limits for premixed flames is hydrocarbon oxidation. For example, the oxidation of PAH precursors such as C_2H_3 inhibits the formation of PAH and thus soot. Oxidation of PAH by O_2 was found to be of secondary importance.

Takahashi and co-workers [5,8] successfully correlated the sooting limits for a wide range of fuels by accounting for C-C bonds and flame temperature, and found the fuel molecule structure to be unimportant. Markatou et al. [7] performed detailed kinetic calculations and used measurements of premixed flame sooting limits to validate the HACA mechanism of soot formation. Sooting limits in premixed flames furnish rigorous tests of the accuracy of soot-particle inception models since they involve formation, decomposition and oxidation of PAH.

Sooting limits in nonpremixed systems have been observed in both counterflow and coflow diffusion flames. In counterflow flames, limits have been found by varying the strain rate (i.e. the residence time) or by varying the inert supply at a fixed strain rate [9-16]. In coflow diffusion flames, limits have been observed by changing the flame length or by varying the inert supply [11,15]. Addition of inert can decrease the flame temperature and fuel concentration to an extent that the soot inception chemistry is sufficiently slow that soot cannot form.

The role of soot "oxidation" generally is viewed differently in premixed and nonpremixed flames. Soot oxidation in nonpremixed systems is normally thought to occur on the oxidizer side of the flame sheet and generally is not considered to be critical to soot inception since very little oxygen leaks through the flame front into the soot formation region. Oxygen can appear on the fuel side of coflow flames if it leaks through the quenched base region [2,17], but herein we restrict our attention to oxygen that is intrinsic with the fuel side. The difference in oxygen concentrations in the soot-forming regions of premixed and nonpremixed flames results in a different temperature dependence. Increasing temperature suppresses soot formation in premixed flames and promotes soot formation in nonpremixed flames [2,5]. In premixed flames,

increased temperature favors oxidation chemistry, both for fuel and precursors, over soot formation chemistry. In nonpremixed systems this competition between oxidation and formation does not exist since little oxygen is present on the fuel side.

Despite the differences between soot inception in premixed and nonpremixed flames, the C/O ratio (albeit the local C/O ratio) is shown here to be relevant to sooting limits in diffusion flames. Du and Axelbaum [11] employed the C/O ratio to explain their observations of so-called permanently-blue flames [14]. The fundamental point here originates from the same reasoning as to why C/O ratio is relevant in premixed flames. The simplistic but insightful reasoning is as follows. Consider the stoichiometry of:

$$C_nH_m + (n/2)\, O_2 \rightarrow n\, CO + (m/2)\, H_2\,. \qquad (1)$$

When the C/O ratio is unity there is exactly enough oxidizer to retain the carbon in the gas phase as CO, while a higher C/O ratio can lead to soot formation. If the products are instead assumed to be CO and H_2O the sooting limit can be expressed in terms of an effective equivalence ratio [5] but herein we will consider only the C/O ratio. The measured soot limit in premixed ethylene/air combustion occurs around $(C/O)_c = 0.6$ [1,5,6,8] due to finite rate chemistry and the production of H_2O and CO_2. This limiting C/O ratio was found to have only a slight dependence on the amount of N_2 in the oxidizer. As noted earlier, the sooting limits result from a competition between formation and oxidation and Markatou et al. [7] have shown that in premixed flames oxidation of PAH by O_2 is of secondary importance. The critical oxidation that dictates the sooting limits is hydrocarbon oxidation. This explains why simple thermodynamic considerations like that above are valuable in understanding sooting limits.

For nonpremixed systems a similar competition between oxidation and formation may exist on the fuel side because of the presence of oxygen containing species on the fuel side. Du et al. [10] showed that the addition of CO_2 to the fuel side of diffusion flames can suppress soot formation chemically. Several studies have found that soot particle oxidation on the fuel side of a diffusion flame can be significant [3,17,18].

From the above reasoning, the local C/O ratio may be valuable in identifying local conditions wherein there is excessive oxidizer such that soot will not form. Furthermore, it has been shown that soot does not form at low temperatures in nonpremixed flames, with the threshold ranging

from about 1250-1650 K [2,18-20], a temperature referred to here as the critical temperature for soot formation, T_c. We thus propose that for soot particles to form, two required conditions must occur simultaneously somewhere in the flame: temperature must be above T_c, and the C/O ratio must be above a critical value, $(C/O)_c$. These conditions are presumed to be necessary, but not sufficient, for soot inception because residence time is critical to soot inception in diffusion flames. Short residence times can suppress soot formation but for the microgravity flames considered here the residence times are long.

One can gain insight by considering a simple model of the global flame structure in mixture-fraction space for reaction between a typical fuel (C_2H_4) and O_2, following Refs. [11,21,22]. Mixture fraction, Z, is defined for ethylene-oxygen systems as:

$$Z = [(24/7)Y_{C2H4} - Y_{O2} + Y_{O2,0}] / [(24/7)Y_{C2H4,0} + Y_{O2,0}] \quad (2)$$

where Y denotes mass fraction and subscript 0 denotes conditions in the supply gas. In Eq. (2), Y_{C2H4} and Y_{O2} are linear with respect to Z on the fuel and oxidizer side of the flame, respectively. In the Burke-Schumann limit with unity Lewis number, Y_C, Y_O and T also are linear in Z. Note that the Burke-Schumann limit is only used for clarity, and the essential issues are not dependent on the assumptions of the Burke-Schumann model. Eq. (2) leads to the definition of stoichiometric mixture fraction:

$$Z_{st} = [1 + (24/7)Y_{C2H4,0}/Y_{O2,0}]^{-1} = [1 + 3X_{C2H4,0}(1/7 + 1/X_{O2,0})]^{-1} \quad (3)$$

where X is mole fraction.

Figure 1 makes use of the above model to explain the role of C/O ratio and temperature in unstrained nonpremixed systems. This figure depicts two diffusion flames with $Z_{st} = 0.226$. First consider a diffusion flame of pure C_2H_4 and O_2 indicated by the dotted line. In contrast to premixed flames, both C/O and T vary rapidly on the fuel side of diffusion flames. For purposes of discussion, we will assume that $T_c = 1250$ K and $(C/O)_c = 1$. As indicated by the hatched line, a broad region exists where both $T > 1250$ K and $C/O > 1$ on the fuel side of the flame. Thus, there is a broad region wherein conditions are favorable for soot inception, and this flame should produce soot given sufficient residence time. Consider next the other flame in Fig. 1, where both ethylene and oxygen have been diluted with nitrogen such that Z_{st} is held fixed but now the temperature has been reduced such that C/O = 1 where T = 1250 K on the fuel side. There is no

change in the curve of C/O ratio but it is clear that the structure of the flame vis-à-vis temperature and C/O ratio is very different. In fact, this characterizes a flame at the sooting limit since it has an infinitely thin region with C/O $\geq$ 1 and T $\geq$ 1250 K. Thus either the kinetics of soot inception are too slow (since T < 1250 K) or the oxygen content is sufficiently high that the carbon will be tied up in the gas phase (C/O < 1). There are great simplifications in this reasoning, but these concepts serve to motivate this study.

The emphasis of this work is not soot growth and oxidation, which can be strongly affected by convection direction, but soot inception, which is less dependent on convection direction because it involves gas phase chemistry. Nonetheless, the role of convection direction will be evaluated in this work and is one motivation for the present spherical geometry. Convection direction affects soot growth and oxidation because soot kinetics are relatively slow, and soot particles typically follow the flowfield. For flow from oxidizer to fuel, particles formed nearest the flame sheet are transported into ever richer regions where they undergo surface growth. The rapid fall-off in temperature and the high activation energy of soot chemistry will limit most of the particle inception to the region nearest the flame sheet, as has been observed in counterflow flames where the convection direction is toward the fuel [23]. If instead the direction of convection is from fuel to oxidizer, soot particles that form are quickly transported into leaner conditions where soot oxidation can occur. This resembles what happens along the centerline of a normal coflow flame where soot particles form and are convected through the flame tip into the oxidizer. Chung and co-workers [15,16] coined the terms soot formation flame and soot formation-oxidation flame to differentiate between the two convection directions.

Burner stabilized spherical microgravity flames are employed in this work for two main reasons. First, this configuration offers unprecedented control over convection direction. Second, in steady state these flames are strain-free and thus can yield intrinsic flame characteristics, similar to the way premixed flames have provided intrinsic C/O ratios associated with soot inception limits.

Experimental

The present experiments were conducted in microgravity in the NASA GRC 2.2-second drop

tower. The experimental apparatus is described in detail in Ref. [24], where the present burner again is a 6.4 mm diameter porous stainless steel sphere. All tests were conducted in quiescent ambient gas at 98 kPa (with an estimated uncertainty of ±0.5 kPa). Ignition was performed in microgravity.

The present tests employed three component gases: ethylene, oxygen, and nitrogen. Purity of ethylene was 99.9% while that of oxygen and nitrogen was 99.999%. Gas mixtures were prepared by partial-pressure mixing and have an estimated composition uncertainty of ±0.001 mole fraction. Burner flowrates were established prior to ignition using the mass flowmeter calibration in conjunction with gas-correction factors K_i (0.6, 1 and 1 for C_2H_4, O_2 and N_2, respectively) and the following relationship:

$$\text{(Indicated Flowrate)/(Actual Flowrate)} = 1/K_{mix} = \sum_{i=1}^{2} X_i / K_i \,. \qquad (4)$$

The flowrates were verified periodically with a soap bubble meter. Uncertainties in the flowrates are estimated at ±10%. Burner flowrates were selected such that, regardless of convection direction or degree of dilution, the ethylene consumption rate was 1.51 mg/s for every flame.

The flames were imaged using a color CCD camera with a 16 mm manual-iris lens at f 1.4–4. Spatial resolution was 0.3 mm. Experiments have confirmed that the onset of visible yellow emissions is an effective means of determining soot inception limits in hydrocarbon flames [1,9], and normal-gravity flame testing has confirmed that the present video system is nearly as sensitive as the naked eye to the presence of soot in flames. Sooting limit conditions were defined as conditions for which yellow was evident at drop end but for which a decrease of 0.01 in $X_{C2H4,0}$ or $X_{O2,0}$ (generally whichever is smaller) yielded flames devoid of yellow.

Flame diameters at drop termination were measured based on contours of peak blue intensity. Because some flames were oblong, diameters were determined by averaging the longest chord through each flame and its perpendicular chord. Uncertainties of the flame diameters are estimated at ±5%. Radiative emissions were measured with a thermopile radiometer. Adiabatic flame temperatures were determined using STANJAN 3.8 and neglected radiation and transient conduction losses to the burner. Uncertainties in Z_{st} and T_{ad} arise from uncertainties in gas compositions and are estimated at ± 0.01 and ± 50 K, respectively.

Results and Discussion

The general appearance of the present flames resembles those of previous work in this laboratory [24], although here only flames near sooting limit conditions were considered. All the flames increased in diameter and radiative emissions throughout the 2.2 s drop period, and when yellow emission was observed its intensity diminished with time. Flames where the ejected gas was heavily diluted with nitrogen were generally smaller, brighter, less spherical, and more steady at drop end.

Four representative flames near or at the sooting limits are shown in Fig. 2. Typical of the flames, these images reveal spherical symmetry except near the burner tube. These flames involve convection toward oxidizer (Figs. 2a and 2b) and convection toward fuel (Figs. 2c and 2d). The flames of Fig. 2b and 2d are at the experimental sooting limit since a reduction of 0.01 reactant mole fraction yields blue conditions. Note that soot, when present, appears on the fuel side of the blue flame sheet regardless of convection direction.

As emphasized in Sunderland et al. [24], the present configuration affords unprecedented flexibility in isolating the effects of convection direction and structure. Sixteen sooting limits have been identified and are summarized in Table 1. For both convection directions, the broadest possible range of Z_{st} was sought. As Table 1 shows, there is considerable variation at the sooting limits in flame diameter, d, and burner gas flowrate, m_b.

The sooting limits of Table 1 are presented in Fig. 3 in a plot of O_2 mole fraction in the oxidizer versus C_2H_4 mole fraction in the fuel. This plot allows identification of a regime of blue conditions, defined by the present sooting limit flames. The curve shown is our experimentally-determined boundary of blue conditions, determined from a correlation that will be explained when discussing Fig. 4. There are several interesting trends in the spherical flame data in Fig. 3. As expected, there is a monotonic relationship at the sooting limits between $X_{O2,0}$ and $X_{C2H4,0}$, with a knee bend in the relationship that resembles the shape of a curve of constant T_{ad} [15,16]. Neglecting flames 1 and 2 (see discussion below), within experimental uncertainties convection direction has no detectable impact on the sooting limits. The present spherical flames allow, for the first time, a boundary to be identified between conditions where soot cannot form regardless

of strain rate or residence time (*permanently-blue flames)*, and conditions where soot will form if the strain rate is sufficiently low. Such a boundary cannot be identified conclusively in normal-gravity studies owing to the unavailability of unstrained flows with long residence times.

Figure 3 also includes sooting limits measured in normal-gravity counterflow C_2H_4 flames in three previous studies. Du and Axelbaum [11] considered flames using gas jets of 11 mm separated by 8 mm at various strain rates. Lin and Faeth [14] used a similar burner and similar strain rates. For both of these studies, the flames with measured strain rates of 70 s^{-1} are included here. Hwang and Chung [16] considered C_2H_4 fueled flames in a counterflow apparatus with fuel and oxidizer jets of 14.2 mm diameter separated by 14.2 mm and a fixed global strain rate of 27 s^{-1}. The data of Refs. [11,14,16] fall on the sooting side of the boundary identified in the present microgravity measurements. This is attributed to the strained conditions of the counterflow flames. The Hwang and Chung data have their furthest deviation into the sooting region at high $X_{O2,0}$, possibly because these flames have higher velocities in the soot inception region than do the other counterflow flames shown.

Further insight can be gained by plotting the same limit data in terms of T_{ad} versus Z_{st}, as shown in Fig. 4. This plot is motivated by the following simplified model. Recall in Fig. 1 that $(C/O)_c$ and T_c were used to identify where soot can and cannot form in nonpremixed flames. In other words, if $(C/O)_c$ occurs at the same location as T_c on the fuel side, conditions suitable for soot formation are infinitely thin, indicating a sooting limit. This assumes that the critical temperature is a true limiting condition, which is true only for residence times for which this temperature was determined. Figure 5 reveals a simple relationship between Z_{st} and T_{ad} at the sooting limit. Employing the Burke-Schumann assumption, Y_C, Y_O and T are linear in Z, as in Fig. 1, leading to:

$$C/O = (4/3) Y_C / Y_O = (4/3) (Y_{C,0} / Y_{O,0}) Z / (1 - Z) \tag{5}$$

and, on the fuel side:

$$(T_{ad} - 300 \text{ K}) / (T - 300 \text{ K}) = (1 - Z_{st}) / (1 - Z) . \tag{6}$$

Eq. (3) yields:

$$Z_{st} = [1 + 4 Y_{C,0} / Y_{O,0}]^{-1} . \tag{7}$$

Combining Eqs. (5-7) and replacing T with T_c and C/O with $(C/O)_c$ yields:

$$(T_{ad} - 300\ K) / (T_c - 300\ K) = 1 + Z_{st} [3\ (C/O)_c - 1] . \quad (8)$$

Under the assumption that T_c and $(C/O)_c$ are constants, Eq. (8) predicts a linear relationship between Z_{st} and T_{ad} at the sooting limit. Figure 5 indicates that dramatic increases in T_{ad} are possible for flames at the sooting limit at high Z_{st}.

Considering this, the data in Fig. 3 are replotted in Fig. 4 in terms of Z_{st} and T_{ad}, again defining a region of blue conditions. There are two outliers among the present flames: the two convection-toward-oxidizer flames at the lowest Z_{st} (flames 1 and 2). These are large flames with the lowest burner flowrates considered. These conditions cause large gas-phase radiative losses and large heat losses to the burner. Consequently, flames 1 and 2 are far cooler than their adiabatic flame temperatures would suggest. Indeed, past measurements [24] showed flame 1 to have a peak temperature of 1399 K, not far above the soot formation threshold of 1250 K. Thus flames 1 and 2 are excluded from the data correlation in Figs. 3 and 4 and from the discussion that follows.

Figure 4 shows that the present flames (excepting flames 1 and 2) can be correlated with a straight line, indicating agreement with the simplified model of Eq. (8). A comparison of this correlation and Eq. (8) reveals measured soot formation thresholds of T_c = 1826 K and $(C/O)_c$ = 0.60. The agreement between this value for T_c and the *a priori* value of T_c = 1250-1650 K [2, 18-20] is acceptable given the approximations of the theory, including its assumption of adiabatic flames. The actual flames will be considerably cooler so the true T_c will be less than that predicted when assuming no heat loss. Note that $(C/O)_c$ = 0.60 agrees remarkably well with the typical values observed in ethylene/air premixed flames [1,2,5,6,8]. The slope of this line reveals the profound effect of structure (Z_{st}) on sooting propensity, accounting for a range in T_{ad} at the sooting limit of 1800-2700 K.

Figure 4 provides dramatic evidence that, within experimental uncertainty, convection direction has no measurable effect on the sooting limits of the present flames. The development of Eq. (8) and Figs. 1 and 5 considers structure alone, with no allowance for hydrodynamics. Although it is possible to suppress soot formation by decreasing residence time as in counterflow flames, the present strain-free flames are less affected by residence time, thus leading to structural sooting limits that are more fundamental than others obtained to date. The negligible

effect of convection direction in Figs. 3 and 4 supports this assertion.

The normal-gravity sooting limit flames in Fig. 3 also are included in Fig. 4. Once again, conditions identified as sooting limits in normal-gravity tests would produce yellow flames in the spherical configuration. This is attributed to the intrusion of strain in the normal-gravity tests. We note that the closest agreement between the data of Hwang and Chung [16] and the present sooting limits is near $Z_{st} = 0.4$. For this value of Z_{st}, soot inception occurs near the stagnation plane of the counterflow flame, and residence times can be long.

Figure 5 indicates that the mechanism for attaining a sooting limit may be different at low and high Z_{st}. The flame temperature at the limit condition for the low Z_{st} flame is nearly equal to T_c. Thus, when inert is added to the standard fuel/air flame (low Z_{st}) the limit is attained largely because the temperature is reduced to the extent that the kinetics of soot inception are too slow to produce soot. On the other hand, at high Z_{st} the C/O ratio is high deep into the fuel side of the flame. Thus, the limit is attained because the amount of oxygen on the fuel side of the flame is sufficient to tie up the carbon and keep soot from forming. Farther into the fuel-rich region the amount of oxygen is reduced but the temperature is too low to allow soot formation.

The present flames are limited by the 2.2 s test times and while heat release rate was held constant, the flames had different sizes and flowrates. Some flames may be affected by transient color, transient burner heating, gas-phase radiation, and thermophoretic trapping of soot. These effects are expected to compete in determining the color of the present flames. Furthermore, yellow emissions from the present flames decrease throughout the 2.2-s tests. Transient burner heating and gas-phase radiation are discussed in Refs. [24-26] and both reduce the peak temperatures, particularly for flames with small X_{N2} in the burner gas. Finally, thermophoretic trapping of soot residual from ignition is expected to have no effect for flames with convection toward fuel but could be a factor in flames 1-3.

Conclusions

Sooting limits were studied in spherical microgravity diffusion flames reacting ethylene and oxygen at various levels of dilution. Unlike past measurements of limits in normal-gravity, the

present configuration involves unstrained flames and allows independent variation of Z_{st} and convection direction. The major conclusions are as follows:

1. Sooting limits for the present flames can be successfully correlated in terms of Z_{st} and T_{ad}, where T_{ad} was found to increase linearly with Z_{st}. Previous sooting limits from normal-gravity counterflow tests were found to correspond to conditions that would be yellow in the present tests, which is attributed to the intrusion of strain in the counterflow arrangement.
2. Soot-free conditions were found to be strongly favored with increasing Z_{st}. When T_{ad} is fixed, an increase in Z_{st} leads to a reduction in C/O in the high-temperature zone on the fuel side. This favors blue conditions as a result of competition between oxidation and formation chemistry associated with soot inception.
3. The relationship between adiabatic flame temperature and stoichiometric mixture fraction at the sooting limits was found to be in qualitative agreement with a simple theory based upon the Burke-Schumann approximation and the requirement that soot inception requires temperatures and C/O ratios to be above their critical values.
4. Convection direction had no systematic effect on the observed sooting limits. This is consistent with the simplified theory, predicated on the belief that sooting limits are associated with soot inception, which is largely unaffected by hydrodynamics for the present flames.
5. The mechanisms responsible for sooting limits at low and high Z_{st} are different. In the standard fuel/air flame (low Z_{st}) the limit is attained largely by reducing the temperature until the kinetics of soot inception are too slow to produce soot. On the other hand, at high Z_{st} the limit is attained because the amount of oxygen on the fuel side of the flame is sufficient to tie up the carbon and keep soot from forming. Farther into the fuel-rich region, where the amount of oxygen is reduced, the temperature is too low to allow soot to form.

Acknowledgments

This research was funded by the National Aeronautics and Space Administration under grants NCC3-697 and NAG3-1910 (RLA), and NCC3-696a and NAG3-1912 (BHC). Assistance with the microgravity experiments was provided by Brian Goldstein, Carrie Johnston, and Nathan Diederich. We appreciate the programmatic support provided by Dr. Merrill King and Roger Forsgren.

REFERENCES

1. Haynes, B. S., and Wagner, H. Gg., *Prog. Energy Combust. Sci.* 7:229 (1981).
2. Glassman, I., *Proc. Combust. Inst.* 22:295 (1988).
3. Urban, D. L. and Faeth, G. M., 39th AIAA Meeting, Reno, AIAA 2001-0332 (2001).
4. Revkin, A. C., *The New York Times*, April 21, p. 1 (2001).
5. Takahashi, F., and Glassman, I., *Combust. Sci. Tech.* 37:1 (1984).
6. Harris, M. M., King, G. B., and Laurendeau, N. M., *Combust. Flame* 64:99 (1986).
7. Markatou, P. Wang, H. and Frenklach, M., *Combust. Flame* 93:467 (1993).
8. Takahashi, F., Physical and Chemical Aspects of Combustion: A Tribute to Irvin Glassman, F. L. Dryer and R. F. Sawyer, Eds. Gordon and Breach, Amsterdam, 1997, p. 161.
9. Du, D. X., Axelbaum, R. L., and Law, C. K., *Proc. Combust. Inst.* 22:387 (1988).
10. Du, D. X., Axelbaum, R. L., and Law, C. K., *Proc. Combust. Inst.* 23:1501 (1990).
11. Du, J. and Axelbaum, R. L., *Combust. Flame* 100:367 (1995).
12. Du, D. X., Axelbaum, R. L., and Law, C. K., *Combust. Flame* 102:11 (1995).
13. Sugiyama, G., *Proc. Combust. Inst.* 25:601 (1994).
14. Lin, K. –C. and Faeth, G. M., *J. Propulsion and Power* 12:691 (1996).
15. Kang, K. T., Hwang, J. Y., Chung, S. H., and Lee, W., *Combust. Flame* 109:266 (1997).
16. Hwang, J. Y. and Chung, S. H., *Combust. Flame* 125:752 (2001).
17. Kaplan, C. R. and Kailasanath, K. *Combust. Flame* 124: 275 (2001).
18. Sunderland, P. B. and Faeth, G. M., *Combust. Flame* 105:132 (1996).
19. Santoro, R. J., Yeh, T. T., Horvath, J. J., and Semerjian, H. G., *Combust. Sci. Technol.* 53:89 (1987).
20. Glassman, I., *Proc. Combust. Inst.* 27:1589 (1998).
21. [illegible] Menlo Park, 1985, p. 85

Flame	Ambience	$X_{C2H4,0}$	$X_{O2,0}$	m_b, mg/s	Z_{st}	T_{ad}, K	d, mm
1	Oxidizer	1.00	0.21	1.51	0.064	2347	28.7
2	Oxidizer	0.60	0.20	2.51	0.098	2254	31.4
3	Oxidizer	0.31	0.17	4.86	0.151	2006	32.4
4	Oxidizer	0.18	0.28	8.37	0.333	2280	29.9
5	Oxidizer	0.17	0.29	8.86	0.353	2283	29.3
6	Oxidizer	0.11	0.50	13.7	0.586	2360	22.5
7	Oxidizer	0.11	0.80	13.7	0.685	2525	16.4
8	Oxidizer	0.15	1.00	10.0	0.660	2768	11.6
9	Fuel	1.00	0.13	35.4	0.041	1851	17.5
10	Fuel	0.80	0.13	35.4	0.051	1840	20.3
11	Fuel	0.60	0.13	35.4	0.066	1822	21.8
12	Fuel	0.21	0.25	18.7	0.277	2248	29.6
13	Fuel	0.19	0.30	15.7	0.335	2348	28.3
14	Fuel	0.15	0.50	9.69	0.509	2538	27.5
15	Fuel	0.12	0.80	6.30	0.666	2583	25.9
16	Fuel	0.13	1.00	5.17	0.692	2690	25.0

Table 1. Sooting limit conditions for burner-stabilized spherical nonpremixed flames in microgravity. Ambient pressure is 98 kPa throughout.

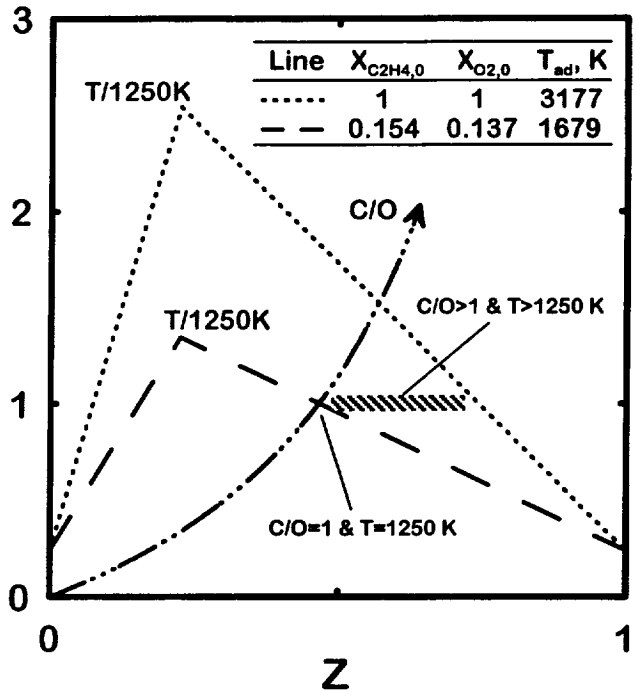

Fig. 1. Effect of T_{ad} on soot formation for constant Z_{st} in the Burke-Schumann limit. Z_{st}=0.226 for both flames.

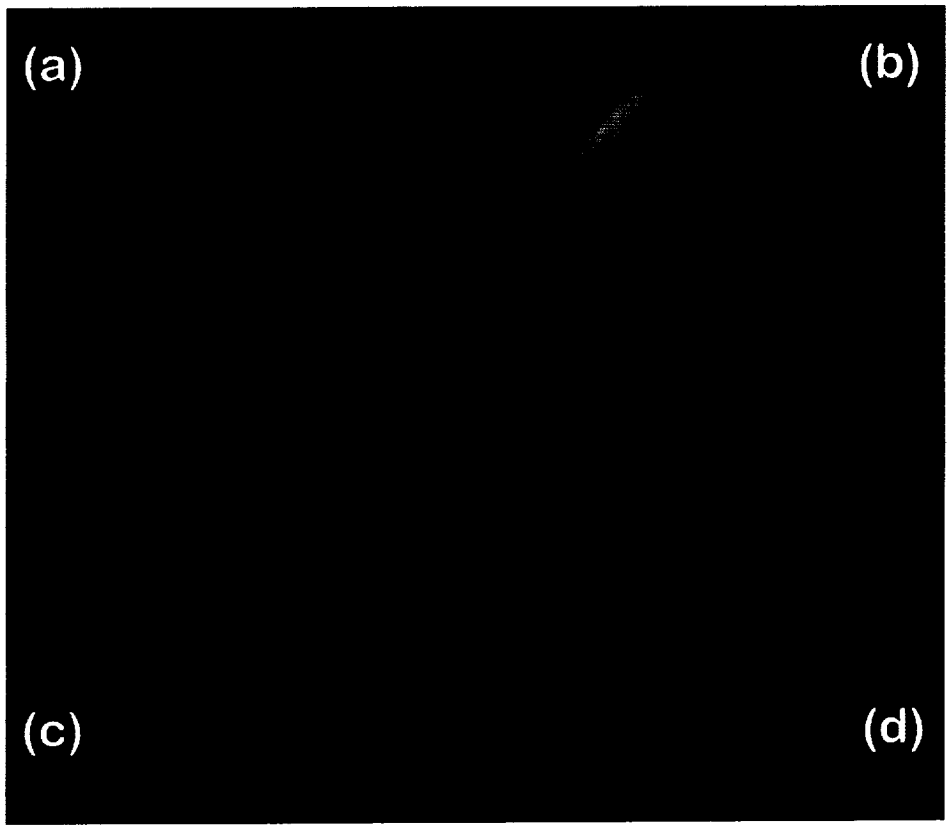

Fig. 2. Representative flames below the sooting limit (a and c) and at the sooting limit (b and d) for convection toward oxidizer and convection toward fuel. Conditions are (a) 18% C_2H_4 flowing into 27% O_2, (b) into 28% O_2, (c) O_2 flowing into 12% C_2H_4, and (d) into 13% C_2H_4. Flames (b) and (d) correspond to flames 4 and 16 in Table 1. Images are from just before drop termination.

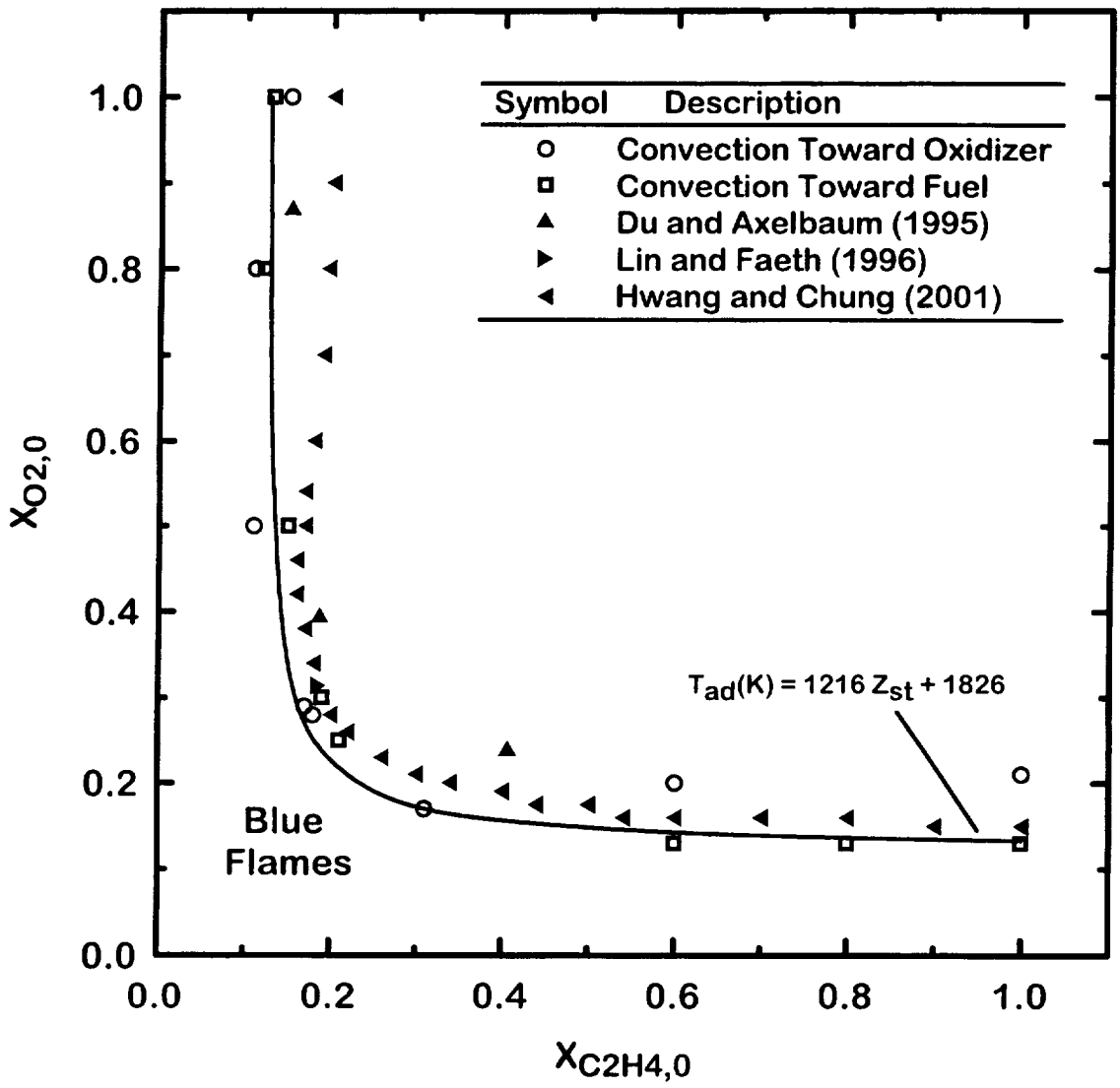

Fig. 3. Oxygen mole fraction versus ethylene mole fraction in the supply gases for the present sooting limit flames and for published normal gravity limit flames [11,14,16]. The curve arises from the data fit of Fig. 4.

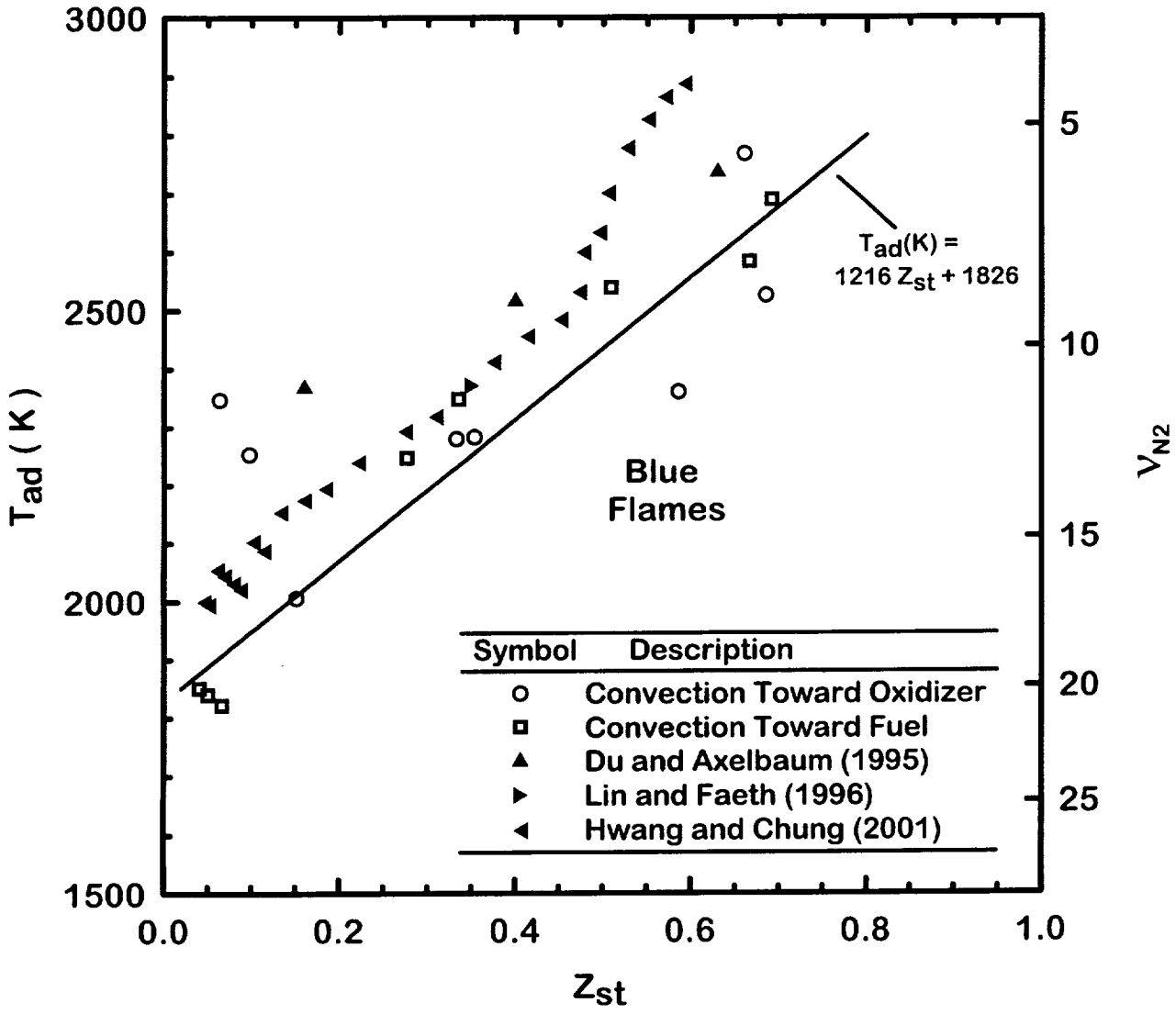

Fig. 4. Adiabatic flame temperature versus stoichiometric mixture fraction for the present sooting limit flames and for published normal gravity limit flames [11,14,16]. The line is a least-squares fit to the present data excluding flames 1 and 2 and is described by the equation shown. The symbol ν_{N2} is associated with the stoichiometry of $C_2H_4 + 3O_2 + \nu_{N2}N_2 \rightarrow$ products, and corresponds with T_{ad} as shown.

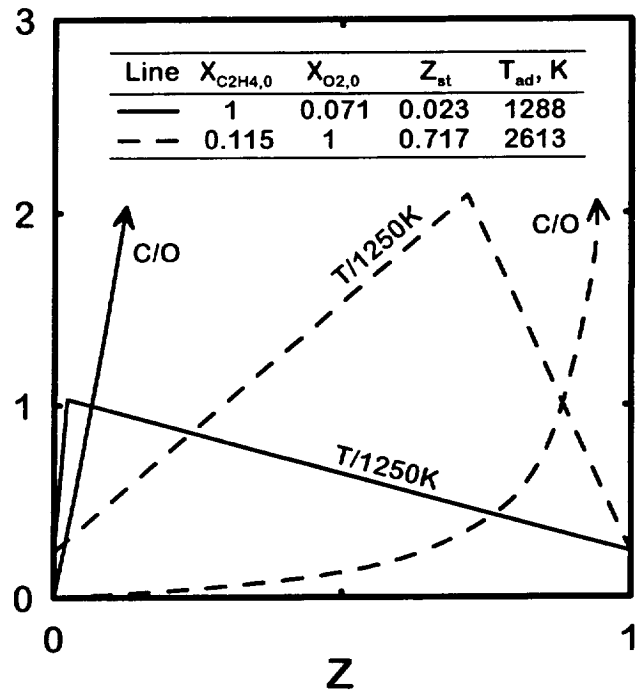

Fig. 5. Effect of Z_{st} on sooting limits in the Burke-Schumann approximation. Two representative flames are shown at the sooting limits, one at low Z_{st} and one at high Z_{st}.